PERGAMON

Journal of Structural Geology 22 (2000) 259–276

JOURNAL OF STRUCTURAL GEOLOGY

www.elsevier.nl/locate/jstrugeo

Progressive lattice misorientation and microstructural development in quartz veins deformed under subgreenschist conditions

Osamu Nishikawa [a,*], Toru Takeshita [b]

[a] *Institute of Geology and Paleontology, Graduate School of Science, Tohoku University, Sendai, 980-8578, Japan*
[b] *Department of Earth and Planetary Systems Science, Hiroshima University, Higashi-Hiroshima, 739-8526, Japan*

Received 9 December 1998; accepted 14 September 1999

Abstract

Progressive microstructural changes in quartz veins which were moderately deformed under subgreenschist conditions have been investigated by observation of microstructures and crystallographic orientation analysis. The geometry of kink bands relative to the finite strain framework and systematic dispersion patterns of crystallographic orientations of subgrains and recrystallized grains suggest the dominant and subordinate operation of basal $(0001)\langle a\rangle$ and $\langle m\rangle$, and ω $\{10\bar{1}3\}\langle a\rangle$ slip systems, respectively, in the deformed quartz. Deformation of the quartz at an early stage was dominated by the formation of kink bands which rotated quickly and locked up at an inclination angle, α, of the active slip plane relative to the compression axis exceeding the optimum angle for slip ($\alpha = 45^\circ$). Subsequently, polygonization and subgrain rotation recrystallization occurred first in highly strained portions, such as the inside of kink bands, and then outside of them. The sequential deformation process is reflected in the transition of the crystallographic orientation distribution from systematic to complicated (or random) dispersion patterns. Based on the fact that the subgrains and recrystallized grains are always elongated perpendicular to the bulk shortening axis, without any control of the orientation of active slip plane or kink bands, it is concluded that the polygonization and recrystallization by subgrain rotation were caused by a complete rearrangement of dislocation configuration by climbing, independent of kinking.

1. Introduction

In middle-upper crustal conditions, a main ductile deformation mechanism in quartz is intracrystalline plasticity which proceeds through the movement and the multiplication of dislocations. These processes are controlled by physical conditions such as temperature and strain rate, and magnitude of strain, which are sensitively reflected in deformation microstructures and crystallographic orientation distributions (COD) of quartz (e.g. Tullis et al., 1990; Hirth and Tullis, 1992; Gleason et al., 1993).

In high-temperature dislocation creep, the operation of multiple slip systems in quartz makes it possible to strain homogeneously, whereas, at lower greenschist (subgreenschist) facies conditions, deformation of quartz is highly anisotropic because limited slip systems are activated. Plastic anisotropy in quartz has been documented for naturally deformed quartzite (e.g. Bouchez, 1977; Takeshita et al., 1999) and theoretically predicted by Takeshita and Wenk (1988). Kink bands are a typical microstructure in quartz deformed under such low temperature deformation conditions. Nishikawa and Takeshita (1999) have shown how the yielding stress for kinking and morphological features of kink bands, such as their symmetry and width, vary with the orientation of the active slip plane (basal plane) relative to the compression axis in quartz. The mechanical behaviour of quartz is also affected by recovery and dynamic recrystallization processes. Under low temperature and high strain rate conditions, recovery is not pervasive in quartz because diffusion processes (i.e. dislocation climb) are sluggish, which leads to a significant strain hardening (e.g.

* Corresponding author.
E-mail address: nisikawa@dges.tohoku.ac.jp (O. Nishikawa).

0191-8141/00/$ - see front matter
PII: S0191-8141(99)00147-9

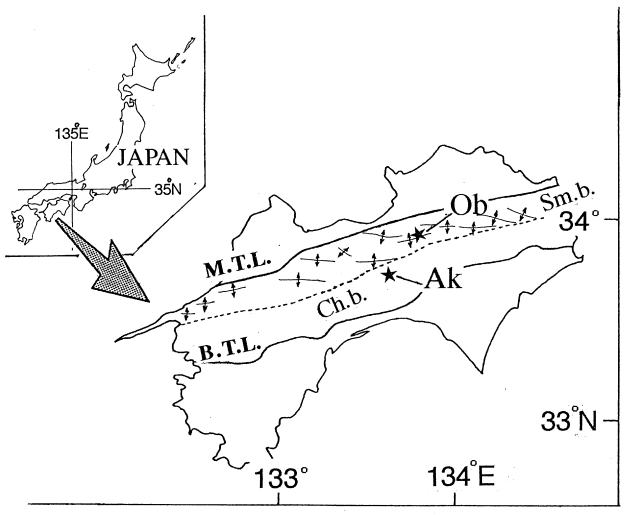

Fig. 1. Map showing sample localities, Ob: Oboke, Ak: Akaragi pass. Axial traces of antiform of the D_3 phase fold are shown by thin lines with arrows. Sm.b.: Sambagawa belt, Ch.b.: Chichibu belt, M.T.L.: Median Tectonic Line, B.T.L.: Butsuzo Tectonic Line.

Nicolas and Poirier, 1976). With increasing temperature and decreasing strain rate, dislocation climbing becomes easier, leading to the operation of recovery and rotation recrystallization. As a result, a rather constant flow stress is maintained and large strain can be achieved.

Due to the recent development of the measurement techniques of crystallographic orientations using the scanning electron microscope (SEM), such as SEM-EBSP (electron back-scatter pattern) and SEM-ECP (electron channeling pattern), increasing attention has been given to lattice misorientation processes in deformed and recrystallized quartz (e.g. Lloyd and Freeman, 1991, 1994; Trimby et al., 1998; van Daalen et al., 1999). Lloyd and Freeman (1991, 1994) showed fairly systematic dispersion patterns of crystallographic orientations of subgrains and recrystallized grains in a quartz porphyroclast, which resulted from subgrain rotation controlled by active slip systems. Lloyd et al. (1992) revealed the pervasive development of Dauphiné twinning in deformed quartz grains in a shear zone and suggested that this may be an important deformation mechanism in quartz. Trimby et al. (1998) investigated a grain boundary hierarchy, defined as misorientation and domain size and their frequency distribution in a quartz mylonite. These studies showed that the dispersion patterns of crystallographic orientations in deformed and recrystallized quartz grains can provide much important information on the recrystallization mechanisms and the operative slip systems. A combination of the COD analysis with detailed microstructural observation can aid an understanding of deformation and recrystallization processes of quartz.

In this study, we have carried out detailed observations on the geometry of kink bands and recrystallization microstructures in quartz veins deformed under subgreenschist conditions and shown their variation with crystallographic orientations of host grains relative to the compression (or bulk shortening) axis. Subsequently we analyzed the COD in kinked and recrystallized grains using a transmission electron microscope (TEM). Based on the microstructures and COD patterns, we inferred operative slip systems and recrystallization mechanisms, and discussed the evolution process of microstructures in the quartz.

2. Geological setting and sample description

Quartz vein samples were collected from the Sambagawa belt in Oboke area and the northern Chichibu belt in Akaragi pass area in central Shikoku, SW Japan (Fig. 1), both of which experienced the Sambagawa intermediate–high pressure type metamorphism of pumpellyite–actinolite facies conditions

Table 1
The features of quartz in layer-parallel vein and en échelon vein samples

Sample	Layer-parallel vein	En échelon vein
Locality	Oboke (Sambagawa belt)	Oboke (Sambagawa belt); Akaragi pass (Chichibu belt)
Style	Parallel to schistosity; Folded into an open style	Cutting schistosity
Width	2–4 mm	2–4 mm
Deformation phase	D_3 phase	post-D_3 phase
Homogenization temp. of fluid inclusions	190–290°C	150–350°C
Sub-basal deformation lamellae	Scarcely observed	Well developed
Kink bands	Developed	Developed
Recrystallization, grain size	Occur, 45 ± 16 μm	Only occur in type I kink bands, 1.3 ± 0.7 μm
Subgrain size	9.4 ± 6.5 μm	1.6 ± 0.8 μm
Dislocation density	$(2.7 \pm 1.1) \times 10^8$ cm^{-2}	$(1.6 \pm 0.5) \times 10^9$ cm^{-2}

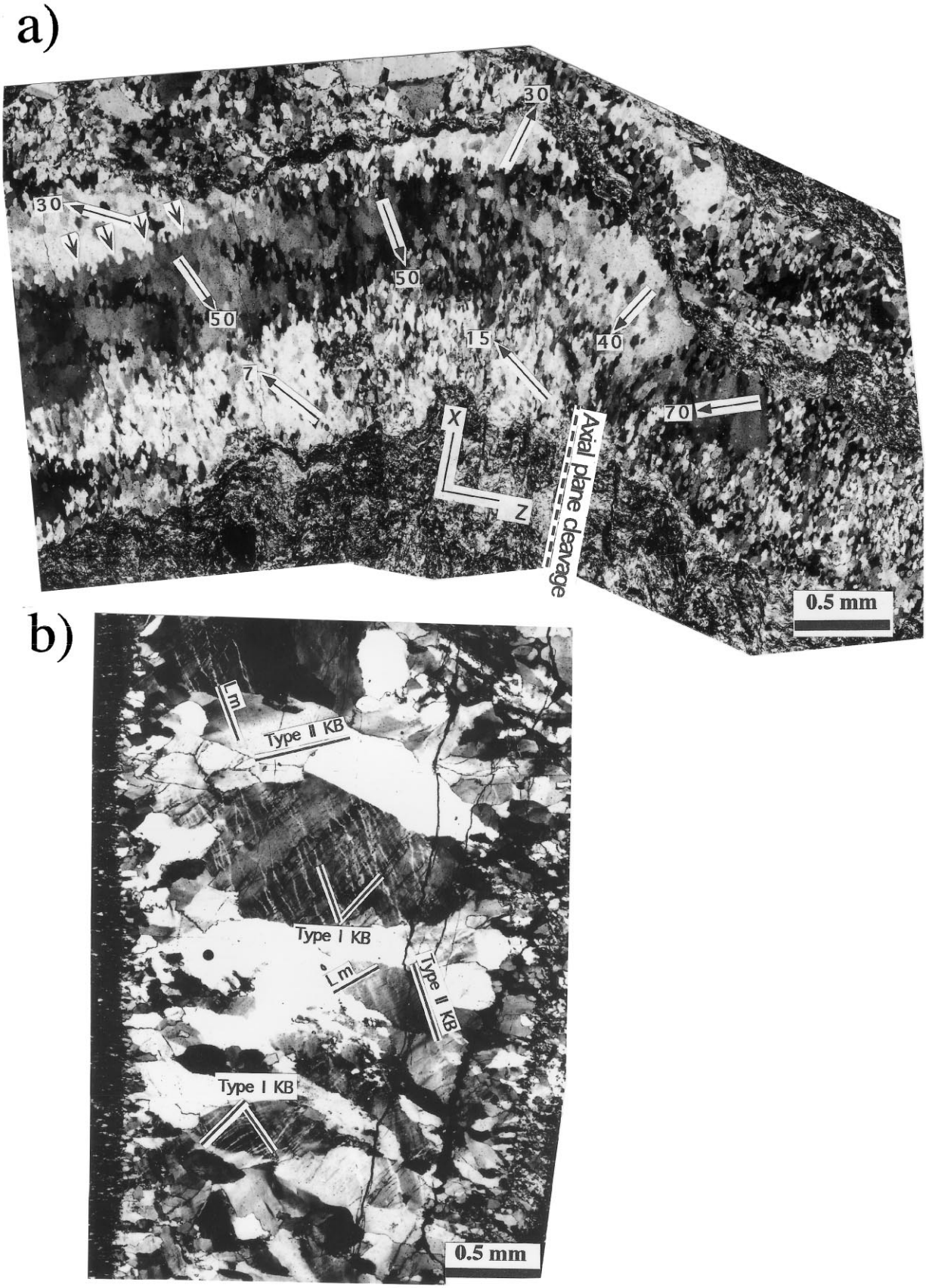

Fig. 2. Optical micrographs (crossed polarizers) of the quartz veins. (a) Layer-parallel vein which is folded and recrystallized by the D_3 deformation. The average *c*-axis orientation in each host domain is shown by an arrow with the number indicating its plunge. Small arrows denote serrated host grain boundaries. *X* and *Z* denote the orientations of the finite elongation and shortening axes, respectively. (b) En échelon vein (after fig. 2 of Nishikawa and Takeshita, 1999). Two types of kink bands (indicated by type I KB and type II KB) and deformation lamellae (indicated by Lm) are developed in the quartz grains.

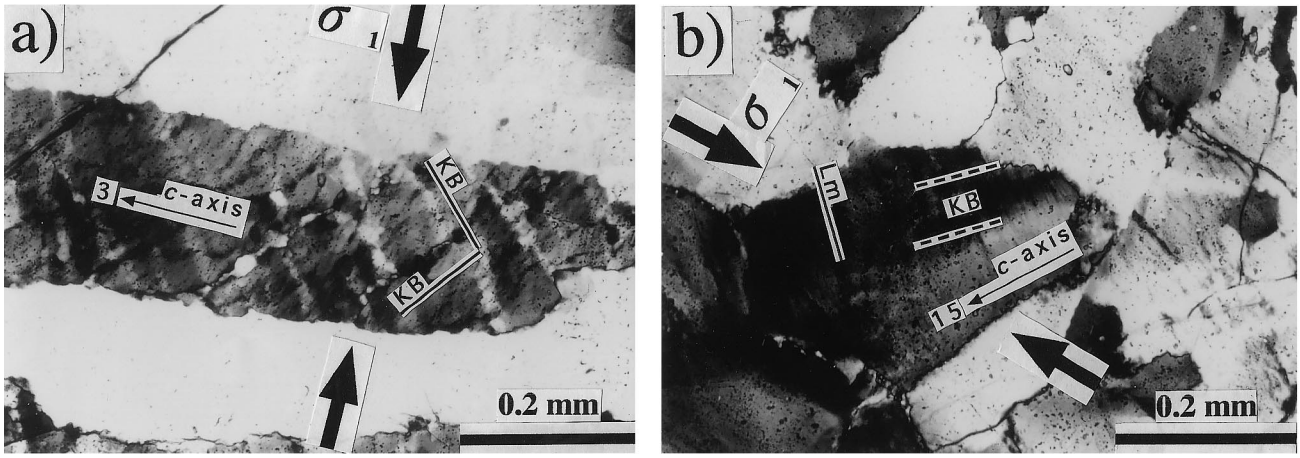

Fig. 3. Optical micrographs (crossed polarizers) showing deformation microstructures in the en échelon quartz veins (after fig. 4 of Nishikawa and Takeshita, 1999). (a) Type I kink bands in a grain compressed parallel to basal (0001) plane. (b) Type II kink bands and sub-basal deformation lamellae in a grain compressed oblique to basal (0001) plane. The *c*-axis orientation in each grain is shown by an arrow with the number indicating its plunge. The compression axis (σ_1) inferred from the arrow method by Nishikawa and Takeshita (1999) is denoted by thick arrows. KB: kink bands, Lm: deformation lamellae.

(e.g. Banno and Sakai, 1989; Kawato et al., 1991), and a large amount of ductile deformation (e.g. Hara et al., 1977, 1992; Faure, 1985; Nishikawa et al., 1994) during the Cretaceous (e.g. Isozaki and Itaya, 1990). Both of the belts experienced a N–S shortening after the exhumation which resulted in the formation of E–W- to NW–SE-trending open folds with vertical axial planes and horizontal axes (Fig. 1; Hijikawa phase: Hara et al., 1977; D_3 phase: Faure, 1985; Nishikawa et al., 1994).

Two types of quartz veins were studied (Table 1). The first type are layer-parallel veins which are intruded parallel to the main schistosity of psammitic rocks in Oboke area. They were folded in an open style during the D_3 phase (Fig. 2a). It was shown by Takeshita and Hara (1998) that the layer parallel veins did not experience the pre-D_3 deformations. The other type is en échelon veins which cut the schistosities of pelitic rocks in Oboke and Akaragi pass areas at a high angle and are not deformed by the D_3 phase folding (Fig. 2b).

Microstructures of the en échelon vein samples have been reported in detail by Nishikawa and Takeshita (1999; Table 1). The quartz grains in the en échelon veins are slightly to moderately deformed (Figs. 2b and 3). Although sub-basal deformation lamellae (Ave'Lallement and Carter, 1971) and kink bands are pervasively developed in the quartz grains, recrystallization is limited to highly deformed kink bands. The paleostress orientations during the deformation of the en échelon veins have been determined with both the arrow and c_1–c_2 methods (Carter and Friedman, 1965) by Nishikawa and Takeshita (1999). According to their analysis, the maximum (σ_1) and minimum (σ_3) principal stress axes were oriented parallel to and perpendicular to the vein wall, respectively. The homogenization temperatures of fluid inclusions in the quartz veins range between 150 and 350°C (Takeshita et al., 1997).

For the layer-parallel veins, Hara and Paulitsch (1971) have inferred that the elongation (X), intermediate (Y) and shortening (Z) axes of finite strain during the D_3 phase were parallel to the fold axial plane and normal to the fold axis, parallel to the fold axis and normal to the axial plane, respectively, based on both the 3-D deformed shape and the *c*-axis fabric patterns of recrystallized grains. Recrystallization occurred in layer parallel veins, their grain size ranging from 25 to 65 μm. Approximately 60% of the vein area is recrystallized in a sample shown in Fig. 2(a) and the recrystallization in highly deformed portions such as the interiors of the fold hinges tends to be more pervasive than in the less deformed limbs. The original host grains can often be recognized as domains consisting of the recrystallized grains with similar *c*-axis orientations (Fig. 2a). The average *c*-axis misorientations between neighbouring subgrains and recrystallized grains measured by a U-stage often exceed 25° in the fold inner hinges, but are less than 15° in the fold outer hinges and limbs. In this paper, when the misorientation angle between adjacent recrystallized grains is larger or smaller than 10°, the boundaries are referred to as grain and subgrain boundaries, respectively, according to some previous studies (e.g. White, 1977; Trimby et al., 1998). The host grains often exhibit serrated grain boundaries (indicated by small arrows in Fig. 2a) suggesting the occurrence of grain boundary migration. Although kink bands are pervasively developed, deformation lamellae are rarely found in the layer-parallel veins. Quartz grains in the

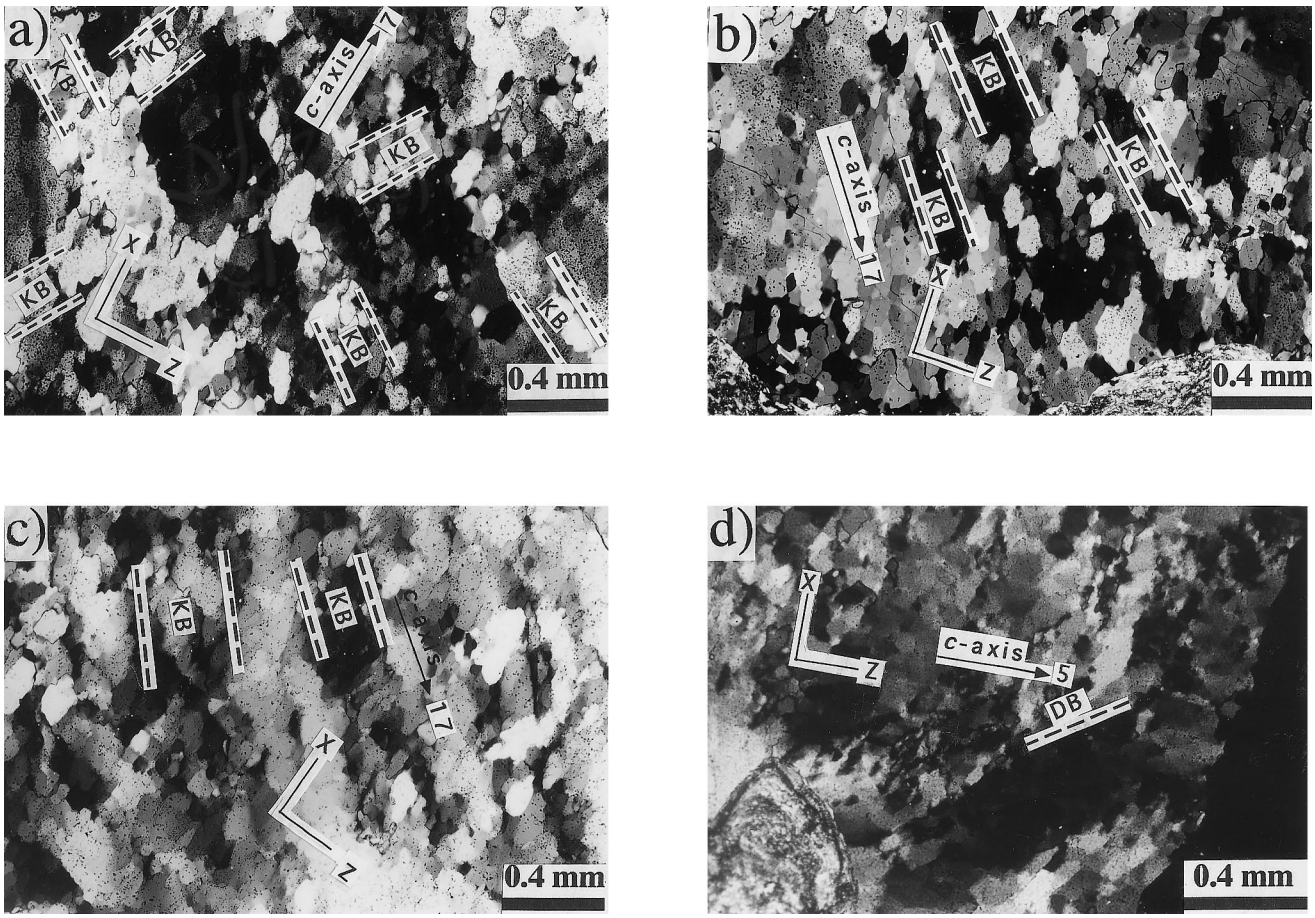

Fig. 4. Optical micrographs (crossed polarizers) showing deformation microstructures in the layer-parallel veins. (a) Type I kink bands in a host grain shortened parallel to basal (0001) plane. Recrystallization is restricted within kink bands. Approximately 50% of the area is recrystallized. (b) Type II kink bands in a host grain shortened oblique to basal (0001) plane. Polygonization and recrystallization occurred throughout the whole host grain. Approximately 40% of the area is recrystallized. (c) Type II kink bands in another host grain shortened oblique to basal (0001) plane. Approximately 60% of the area is recrystallized. (d) A grain shortened perpendicular to basal (0001) plane. The average *c*-axis orientation in each host domain is shown by an arrow with the number indicating its plunge. KB: kink band, DB: domain boundary (see text for details).

layer-parallel veins include numerous fluid inclusions which are often arrayed along subgrain boundaries. The homogenization temperatures of fluid inclusions in the subgrains and recrystallized grains formed during the D_3 phase range between 190 and 290°C in Oboke area (Seki et al., 1993).

3. Microstructural development in deformed host grains with varying crystallographic orientations relative to the shortening axis

Using both an optical microscope and a transmission electron microscope (TEM) (JEOL JEM-2000EX) at an accelerating voltage of 120–200 kV at Hiroshima University, microstructures in both the en échelon and layer-parallel veins have been observed. Here, the inclination angle of the basal plane in quartz relative to the compression (or finite shortening) axis is defined as θ. Microstructures in grains with the three host *c*-axis orientations, perpendicular ($\theta = 0$–10°), inclined ($\theta = 10$–80°) and parallel ($\theta = 80$–90°) to the compression (σ_1) or finite shortening (Z)-axis were analyzed to elucidate the plastic anisotropy.

3.1. En échelon veins

The microstructural features in the en échelon veins have been thoroughly described by Nishikawa and Takeshita (1999), and are briefly summarized here (Table 1). The quartz in the en échelon veins exhibits a strong plastic anisotropy. In grains with *c*-axis oriented perpendicular to the σ_1-axis, very narrow conjugate kink bands (about 1.5–10 μm wide) (type I) tend to develop (Figs. 2b and 3a). In grains with *c*-axis inclined to the σ_1-axis, sub-basal deformation lamellae and monoclinal wide kink bands (10–80 μm) (type II) tend to develop (Figs. 2b and 3b). Boundaries of type

II kink bands are sub-parallel to the *c*-axis. Grains with *c*-axes (sub-)parallel to the compression axis are little deformed. Although subgrains are formed in the whole host grains, recrystallization only occurred in sharply bent type I kink bands, where very fine recrystallized grains (1.3 ± 0.7 μm, ±1 standard deviation) are formed. The subgrain size in grains with either type of kink bands is comparable with the recrystallized grain size. Mean free dislocation densities in grains containing either type of kink bands are fairly high, $1.6 \pm 0.5 \times 10^9$ cm^{-2}.

3.2. Layer parallel veins

3.2.1. Grains with the c-axis perpendicular to the shortening axis

In grains with the *c*-axis oriented perpendicular to the finite shortening (Z) axis (here defined as the direction normal to the axial plane cleavage), conjugate kink bands (type I) symmetrically disposed about the Z-axis are developed (Fig. 4a). Kink band boundaries are rather jagged and the rotation angles of *c*-axis orientation by kinking ranges from 18 to 46°, much larger than those for type II kink bands (described in the following). The width of kink bands ranges between 65 and 180 μm. Recrystallization is pervasive inside the kink bands, but rare outside the kink bands. Therefore, a distinct chess-board pattern consisting of rectangular less recrystallized areas enclosed by four well recrystallized intersecting bands is commonly developed in a deformed host grain (Fig. 4a). Recrystallized grains have an elongate shape with their long and short axes oriented perpendicular to and parallel to the Z-axis, respectively, which is oblique to the orientation of kink bands. In the recrystallized grains, intragranular strain features such as kink bands and undulatory extinction are poorly developed.

3.2.2. Grains with the c-axis inclined to the shortening axis

Polygonization and recrystallization are well developed in these grains (Fig. 4b and c). The size of recrystallized grains (grains with the *c*-axis misoriented more than 10° from the host *c*-axis) is almost the same as that of subgrains (grains with the *c*-axis misoriented less than 10°; Fig. 5). Moreover, the aspect ratios of subgrains and recrystallized grains are constant at around 2.0–2.5, which are independent of their *c*-axis misorientations between neighbouring grains (Fig. 5). Subgrains and recrystallized grains tend to elongate normal to the Z-axis, regardless of the degree of obliquity between the host *c*-axis and Z-axis (Fig. 4b and c).

In moderately deformed host grains where recrystallization is not significant, monoclinal kink bands (type II), whose hinge lines are sub-parallel to their *c*-axes, are preserved (Fig. 4b and c). Unlike the en échelon vein samples, deformation lamellae are rarely found in the host grains. In Fig. 6, the *c*-axis rotation angles of host grains by kinking are plotted versus the mean *c*-axis misorientation angles between neighbouring recrystallized grains (or subgrains) in differently oriented host grains. The *c*-axis misorientation angles between neighbouring subgrains or recrystallized grains show a great variation, ranging from a few degrees up to 90°, while the host *c*-axis rotation angles by kinking are much smaller; ranging between 7 and 18°, independent of the degree of the misorientation

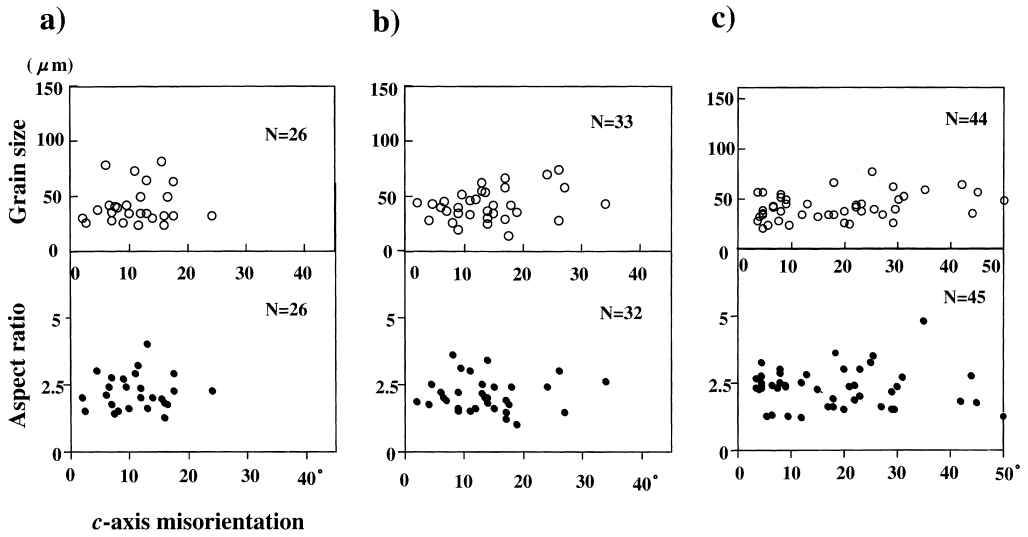

Fig. 5. Diagrams showing grain size (upper box) and aspect ratio (lower box) versus the *c*-axis misorientation angles between neighbouring recrystallized grains or subgrains for three selected host grains from the layer-parallel veins. (a) A polygonized, but little recrystallized host grain. (b) A moderately recrystallized host grain. (c) An extensively recrystallized host grain. N: number of measurements.

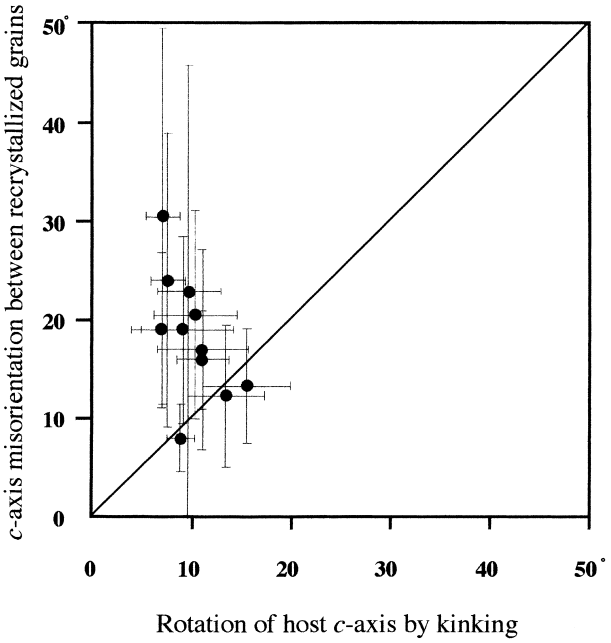

Fig. 6. Diagram showing the mean *c*-axis misorientation angles between neighbouring recrystallized grains or subgrains versus mean host *c*-axis rotation angles by kinking in differently oriented host grains from the layer-parallel veins. For each point, orientations of 20–80 *c*-axes of recrystallized grains or subgrains and 5–10 *c*-axes of kinked host domains are measured. Bars denote a standard deviation (± 1 s.d.)

between subgrains or recrystallized grains. Although the kink bands in host grains are still recognizable in recrystallized grains, intragranular strain features of recrystallized grains are rarely observed under an optical microscope.

3.2.3. Grains with the c-axis parallel to the shortening axis

Microstructures in grains with *c*-axes oriented parallel to the shortening axis are shown in Fig. 4(d). The host grains are inhomogeneously bent and separated into domains with slightly different crystallographic orientations. Sizes and shapes of misoriented domains are rather inhomogeneous. It is worth mentioning that in the sample shown in Fig. 4(d), some of the boundaries between the misoriented domains extend in the direction of 35–45° from the host *c*-axis orientation, and hence could be sub-parallel to the rhomb $\{10\bar{1}1\}$ plane. The boundaries are somewhat similar to shear bands formed parallel to the rhomb plane in quartz compressed parallel to *c*-axis orientation, which have been recently reported by van Daalen et al. (1999).

3.2.4. TEM observation

Under the TEM, distinct microstructural differences were not recognized between grains in different crystallographic orientations. Free dislocations are often oriented parallel to the basal (0001) plane (Fig. 7a). The average dislocation density in all grains is $2.7 \pm 1.1 \times 10^8$ cm^{-2}. Subgrain boundaries consisting of parallel arrays of dislocations are frequently developed. Small subgrains misoriented less than 2 or 3 degrees from neighbours are formed in recrystallized grains and even in large subgrains comparable in size to the recrystallized grains (Fig. 7b). The average size of these small subgrains is 9.4 ± 6.5 μm.

4. Analysis of crystallographic orientation distribution (COD)

4.1. Background and procedure of the analysis

It has been confirmed that lattice misorientation by gliding and subsequent rearrangement of edge dislocations follow the rule that the active slip plane normal, slip direction and external (i.e. lattice) rotation axis are mutually perpendicular (e.g. Nicolas and Poirier, 1976). Therefore, the operative slip systems can be inferred from the dispersion patterns of crystallographic orientations in subgrains and recrystallized grains (e.g. Trépied et al., 1980; Lloyd and Freeman, 1991, 1994; Lloyd et al., 1992; Fliervoet and White, 1995; Lloyd et al., 1997). The pole orientations of representative crystal planes of α-quartz are shown in Fig. 8(a), and the potential slip systems in quartz and the angles between the corresponding lattice rotation axis and *a*-, *m*- and *c*-axes are listed in Table 2. For the case that one of the basal (0001)⟨a⟩ slip systems is activated, both basal plane normal (*c*-axis) and slip direction (one of the *a*-axes) are rotated along a great circle around one of the *m*-axes, while the remaining two out of the three equivalent *a*-axes are rotated along a 30° small circle about the common axis. This

Table 2
Predicted rotation patterns of crystallographic orientations due to subgrain rotation associated with each slip system

Slip System	Pole[a]		
	c	*m*	*a*
basal (0001)⟨*a*⟩[b]	90°	0°, 60°	30°, 90°
basal (0001)⟨*m*⟩[b]	90°	30°, 90°	0°, 60°
$\omega\{10\bar{1}3\}\langle a\rangle$	67°	62°, 23°	37°, 90°
$\omega'\{01\bar{1}3\}\langle a\rangle$	67°	62°, 23°	37°, 90°
$\pi\{10\bar{1}2\}\langle a\rangle$	58°	32°, 65°	43°, 90°
$\pi'\{01\bar{1}2\}\langle a\rangle$	58°	32°, 65°	43°, 90°
rhomb $r\{10\bar{1}1\}\langle a\rangle$	38°	52°, 72°	58°, 90°
rhomb $z\{01\bar{1}1\}\langle a\rangle$	38°	52°, 72°	58°, 90°
prism $\{10\bar{1}0\}\langle a\rangle$	0°	90°	90°

[a] Each pole is rotated along either a great or a small circle about a common axis denoted by 0°. Angular distance of each pole from the rotation axis is shown by degrees.

[b] $\langle a\rangle = \langle 11\bar{2}0\rangle$ $\langle m\rangle = \langle 10\bar{1}0\rangle$.

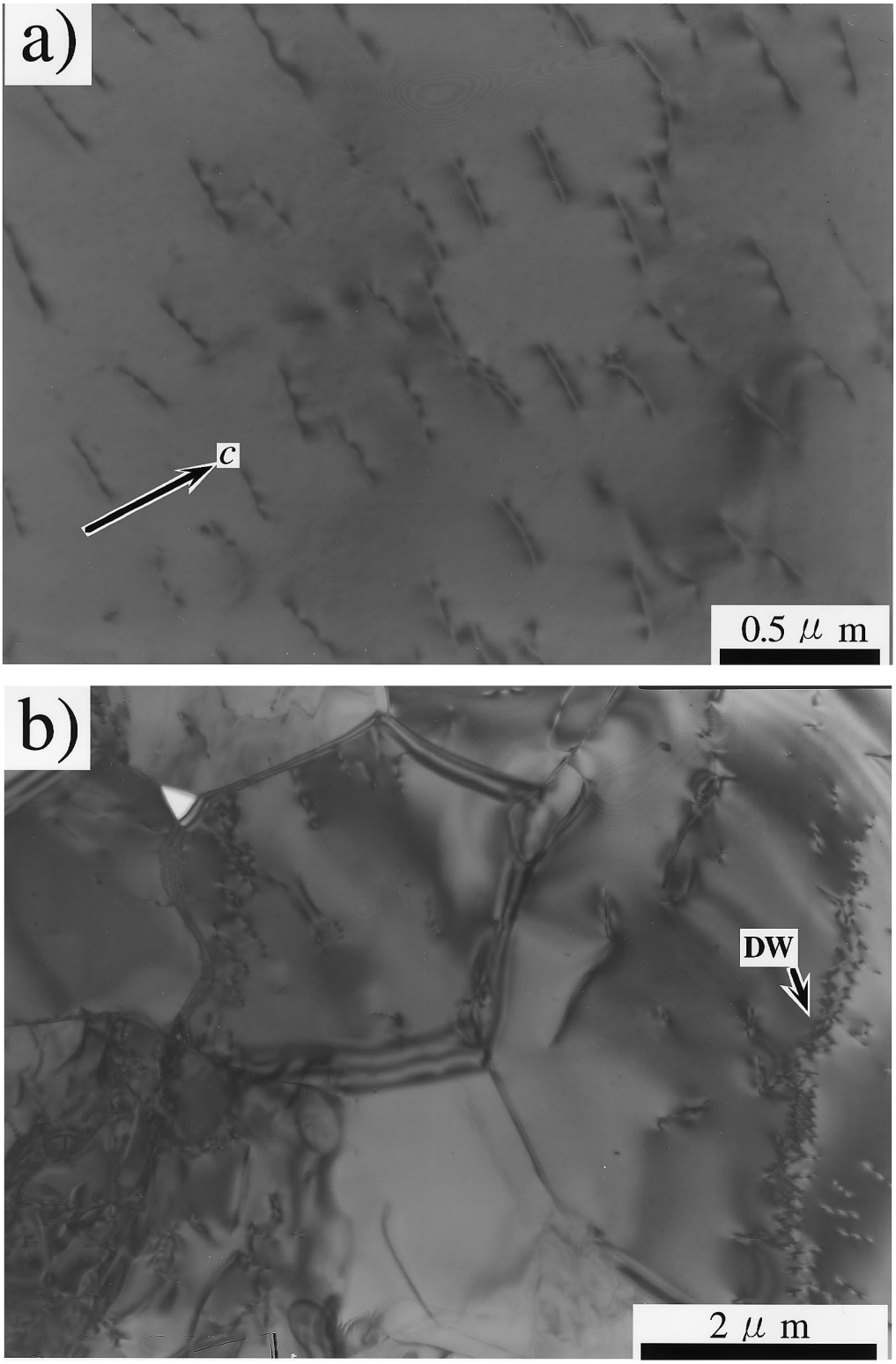

Fig. 7. (a) A TEM bright field image of free dislocations in quartz from the layer-parallel veins. (b) A TEM bright field image of small subgrains in quartz from the layer-parallel veins. DW: dislocation wall. Arrow indicates orientation of the crystallographic *c*-axis.

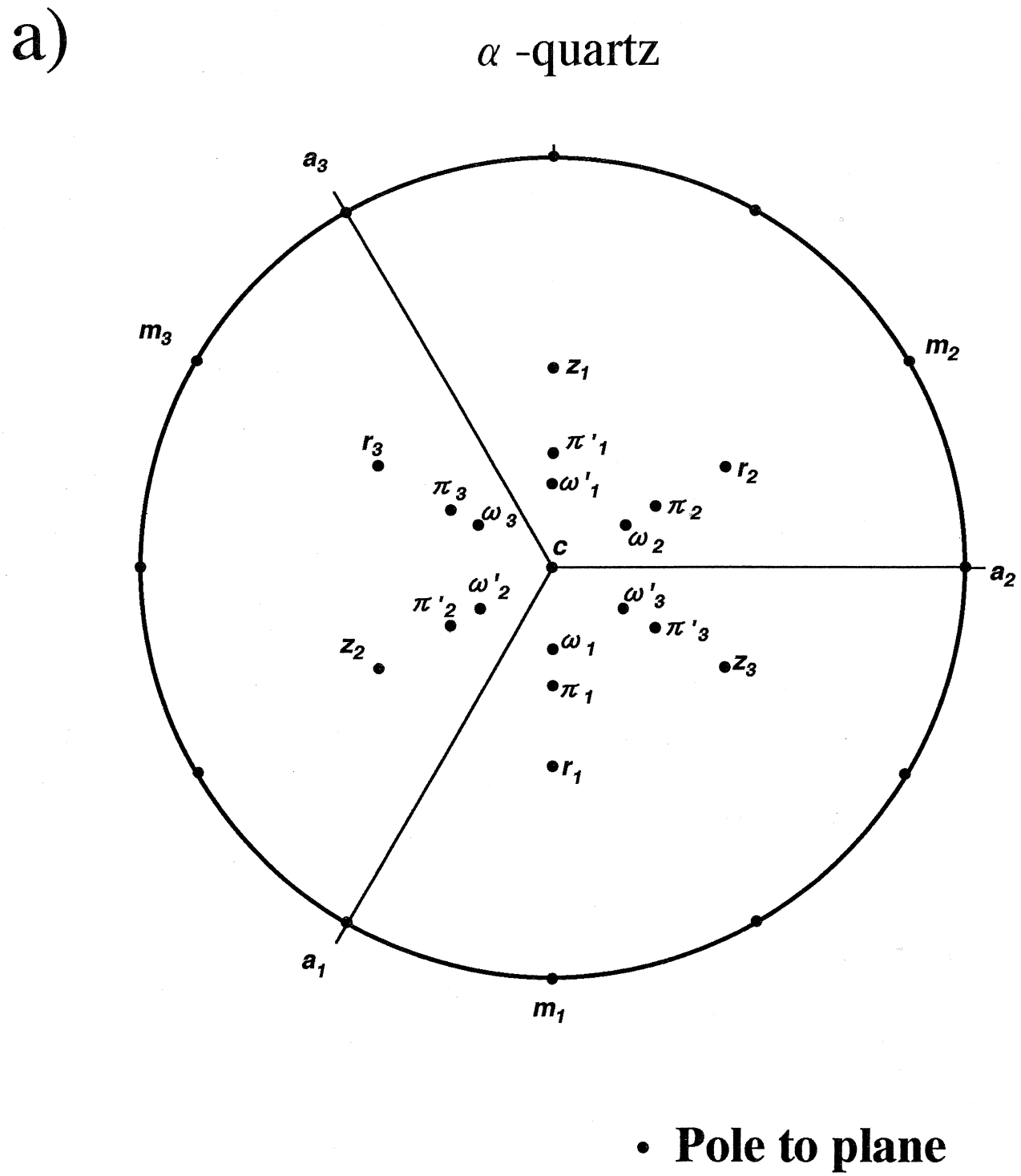

Fig. 8. Stereographic lower-hemisphere projections of crystallographic orientations of subgrains and recrystallized grains in each host grain listed in Table 3. (a) Stereographic lower-hemisphere projections of poles to representative crystal planes in α-quartz listed in Table 2. (b) Samples showing a single systematic dispersion pattern. (c) Samples showing composite dispersion patterns (top row) which can be resolved into at least two dispersion patterns (middle and bottom rows). (d) Samples showing complicated or random dispersion patterns. The best fit great and small circles around a rotation axis for the dispersion of *c*- and *a*-axis orientations are shown by solid lines. Numbers indicate angular distances of each small and great circle from the rotation axis. The inferred active slip system is indicated below each diagram. For solid and dashed lines in *E*-5, *L*-1 and *L*-2 (b), and in *L*-4 and *L*-5 (d), see text for detailed explanations.

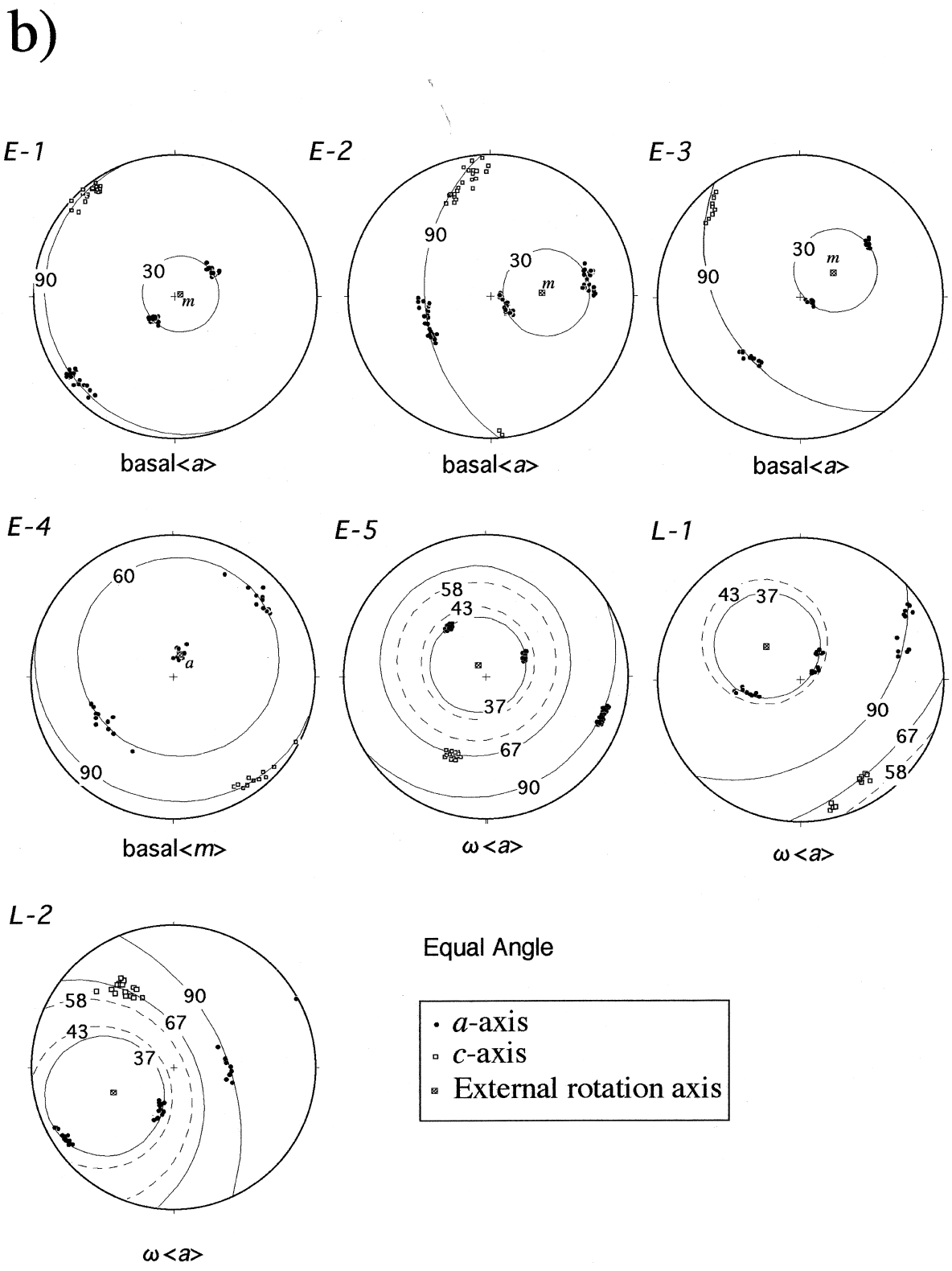

Fig. 8 (*continued*)

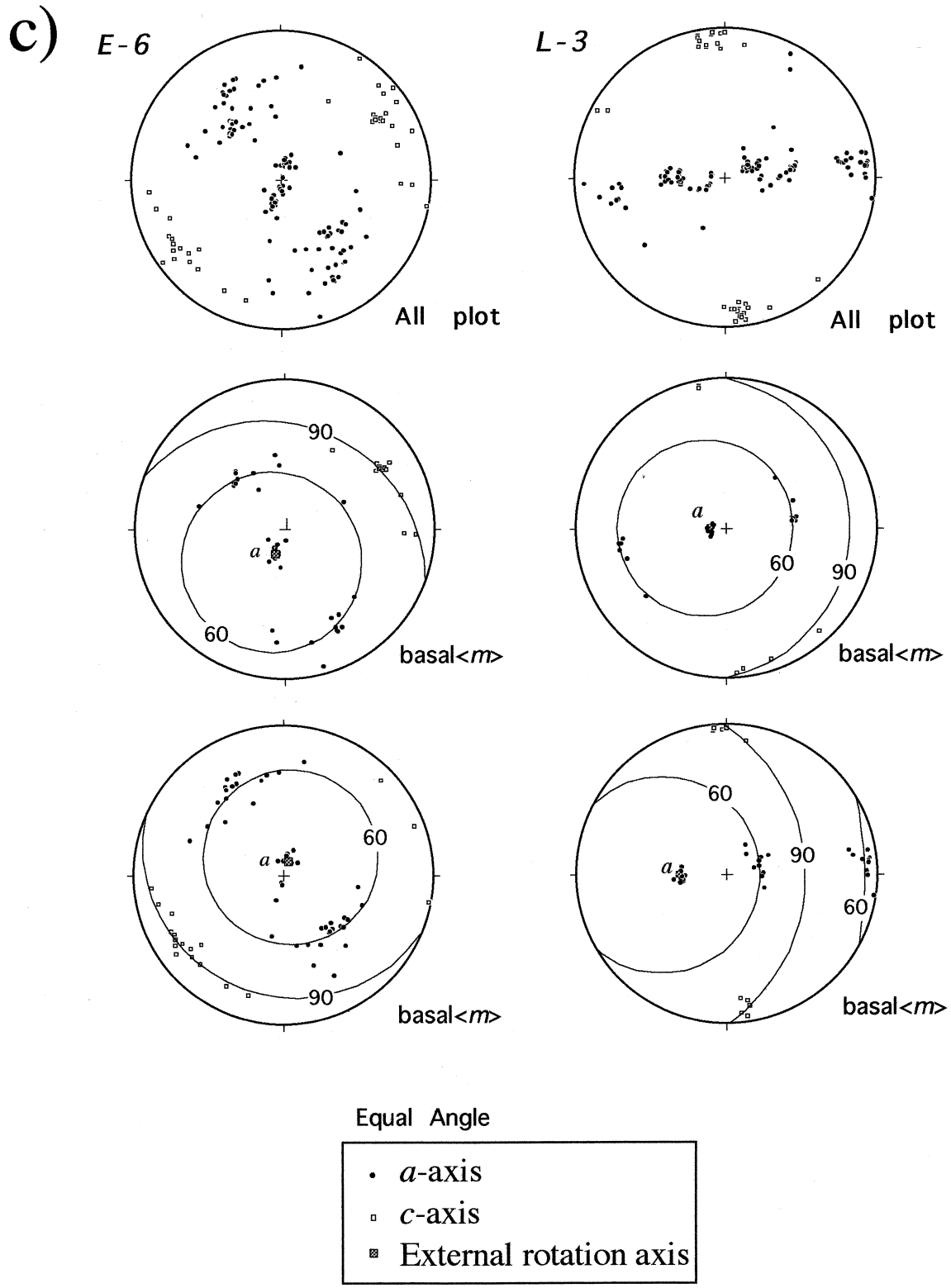

Fig. 8 (*continued*)

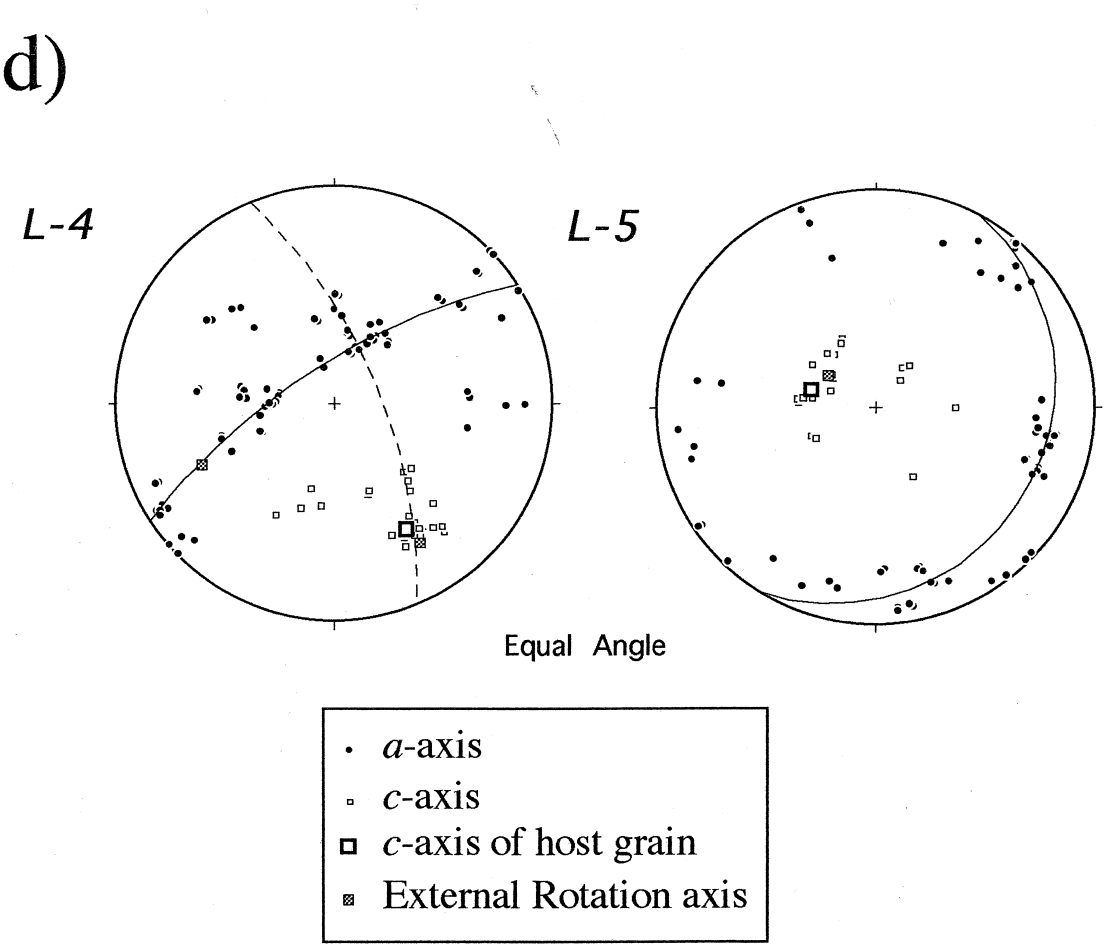

Fig. 8 (*continued*)

rotation pattern analysis has been called the 'dispersion pattern' approach (e.g. Lloyd and Freeman, 1991, 1994).

We have applied the technique for the deformed quartz from both the en échelon and layer-parallel vein samples (Table 3). The crystallographic orientations of quartz were determined by electron diffraction patterns using a TEM with the double-tilt

Table 3
List of the samples used in the analysis of crystallographic orientation distribution

Vein	Sample	c-axis $\wedge$ σ_1[a]	Kink bands	Recrystallization	Dispersion pattern of lattice orientation and inferred active slip systems
En échelon	*E*-1	⊥	Type I	Inside of kink bands	Single, basal ⟨*a*⟩
	E-2	⊥	Type I	Inside of kink bands	Single, basal ⟨*a*⟩
	E-3	O	Type II	None	Single, basal ⟨*a*⟩
	E-4	O	Type II	None	Single, basal ⟨*m*⟩
	E-5	O	Type II	None	Single, ω⟨*a*⟩
	E-6	O	Type II	Weak	Composite, basal ⟨*m*⟩
Layer-parallel	*L*-1	O	Type II	None	Single, ω⟨*a*⟩
	L-2	P	Irregularly bent	Irregular	Single, ω⟨*a*⟩
	L-3	P	Irregularly bent	Irregular	Composite, basal ⟨*m*⟩
	L-4	O	Unknown	Extensive	Random
	L-5	⊥	Unknown	Extensive	Random

[a] O, Oblique; ⊥, Perpendicular; P, Parallel.

specimen holder. It is difficult to distinguish between *r* and *z* orientations by this method, which is performed without quantitative measurement of the intensities of the rhomb reflections. Therefore, the symmetry of quartz crystal in this study was effectively treated as hexagonal (e.g. Fliervoet and White, 1995).

The measurement of crystallographic orientations proceeds as follows. First, quartz grains suitable for the analysis are selected in thin section: those with *c*-axes either in low or high angles to the plane of the thin section. By tilting the specimen holder, either the *a* (or *m*) or the *c*-axis of a specimen is rotated parallel to the beam direction, where either orthogonal or hexagonal diffraction patterns are obtained. In this way the crystallographic orientation with respect to sample coordinates is uniquely identified, which is read from the rotation angles of the specimen holder. The measurement error with this method is within 2–3°, mostly arising from the difficulty of aligning precisely either the *a* (or *m*) or the *c*-axis to the beam direction. The fitting of orientation data to either a great or small circle was carried out by the least squares method.

4.2. Results of the analysis

The COD of subgrains and recrystallized grains in each sample are shown in Fig. 8(b, c, and d). The en échelon and layer-parallel vein samples are denoted by capital letters *E* and *L* preceding the numbers, respectively (Table 3). The lattice dispersion patterns suggesting the activation of a single slip system were mostly obtained in unrecrystallized, kinked host grains from the en échelon veins. In samples *E*-1, 2 and 3, *c*-axes and one of the *a*-axes disperse along a great circle whose pole is oriented in the direction of an *m*-axis, and the other two out of the three crystallographically equivalent *a*-axes disperse along a 30° small circle around the *m*-axis. This distribution pattern suggests the sole operation of one of the basal $\langle a \rangle$ slip systems. In sample *E*-4 the varying *c*-axis orientations lie on a great circle perpendicular to one of the *a*-axes whose orientations vary little, while the other two equivalent *a*-axes are rotated along a 60° small circle around the *a*-axis. This pattern suggests the sole operation of one of the basal $\langle m \rangle$ slip systems.

In samples *E*-5, *L*-1 and *L*-2, the rotation axis of each lattice dispersion lies on a second-order prism plane $(1\bar{1}20)$ and deviates 20–30° from the basal plane, suggesting operation of either $\omega\{10\bar{1}3\}\langle a \rangle$ or $\pi\{10\bar{1}2\}\langle a \rangle$ slip systems. In order to clarify which slip systems operated, the expected dispersion patterns of both *c*- and *a*-axes (i.e. small circles) for one of the $\omega\{10\bar{1}3\}\langle a \rangle$ and $\pi\{10\bar{1}2\}\langle a \rangle$ slip systems are drawn in solid and dashed lines, respectively, around the pole of the best fit great circle for the most variable *a*-axis orientations in each sample (Fig. 8b). Although the *c*-axes and *a*-axes of samples *E*-5, *L*-1 and *L*-2 do not lie exactly on the expected great and small circles for $\omega\langle a \rangle$ slip, it is clear that the dispersion patterns of the different crystallographic axes better fit to the $\omega\langle a \rangle$ than $\pi\langle a \rangle$ slip systems.

Host grains of samples *E*-6 and *L*-3 are highly strained and divided into some domains by kinking and irregular bending, the degree of recrystallization changing from domain to domain. These samples apparently show complicated lattice rotation patterns, which could be a combination of several dispersion patterns (Fig. 8c). In both samples, at least two different dispersion patterns could be identified. The common axis of each dispersion pattern for both samples coincides with an *a*-axis; the *c*-axis and the remaining two *a*-axes are rotated along a great and 60° small circle about the common axis, respectively, suggesting the dominance of basal $\langle m \rangle$ slip. There are many crystallographic orientations which are widely scattered and do not show systematic dispersion patterns suggesting the operation of a certain slip system. These orientations are mostly located in recrystallized domains and not shown in the stereographic plots of the second and third rows in Fig. 8(c).

The COD patterns in recrystallized grains from samples *L*-4 and *L*-5 (Fig. 8d) are rather more complicated than those in unrecrystallized samples. In samples *L*-4 and *L*-5, there could be a tendency for the three equivalent *a*-axis orientations to disperse along a great circle (shown by solid lines in Fig. 8d), suggesting the operation of prism $\langle a \rangle$ slip. On the other hand, in sample *L*-4, a tendency for *c*-axes and one of the three equivalent *a*-axes to disperse along a great circle (shown by a dashed line in Fig. 8d) suggests that basal $\langle a \rangle$ slip might also be recognizable. However, the crystallographic orientations of recrystallized grains are scattered greatly around the host orientations, and hence it is safe to conclude that systematic dispersion patterns cannot be recognized in these samples.

5. Discussion

5.1. Mechanism of dynamic recrystallization and active slip systems in the deformed quartz

The crystallographic orientations of subgrains and recrystallized grains are in general close to those of host grains and show systematic dispersion patterns controlled by the operative slip systems. The degree of misorientation of the recrystallized grains is larger in highly- than in weakly-strained portions (Figs. 2a and 8). Moreover the recrystallized grains exhibit comparable sizes and shapes to those of subgrains (Fig. 5).

These facts suggest that the main recrystallization mechanism in the quartz veins was progressive subgrain rotation. The presence of small subgrains in the recrystallized grains, and even in the large subgrains comparable in size with the recrystallized grains, is indicative of subgrain rotation proceeding with the subsequent deformation and recovery in these grains (Trimby et al., 1998).

On the basis of the geometry of kink bands relative to the finite strain framework, it can be concluded that basal (0001) slip was dominantly activated in both types of the quartz veins. The conclusion is also supported by TEM observations that dislocations are often aligned parallel to the basal plane (Fig. 7a). The dominance of basal slip (both basal $\langle a\rangle$ and basal $\langle m\rangle$) was further inferred from the dispersion patterns of crystallographic orientations of subgrains and recrystallized grains. However, the dispersion pattern suggesting basal $\langle m\rangle$ slip could alternatively have been caused by equal amounts of successive slip parallel to the two adjacent $\langle a\rangle$ directions. In addition to basal slip, the COD patterns suggest slip on the ω $\{10\bar{1}3\}$ plane in the $\langle a\rangle$ direction. Although many authors have reported the dominant activity of both basal $\langle a\rangle$ (e.g. Carter and Friedman, 1965) and $\langle m\rangle$ slip systems (e.g. Lloyd and Freeman, 1991, 1994) and the subordinate activity of both $r\{10\bar{1}1\}$ (or $z\{01\bar{1}1\}$)$\langle a\rangle$ (e.g. Schmid and Casey, 1986; Law et al., 1990) and $\pi\{10\bar{1}2\}\langle a\rangle$ (e.g. Law et al., 1990; Lloyd and Freeman, 1991, 1994) slip systems in natural quartz deformed under subgreenschist or greenschist facies conditions, the activation of $\omega\{10\bar{1}3\}\langle a\rangle$ slip has so far been reported only in an experimentally deformed β-quartz as a subordinate slip system (Baëta and Ashbee, 1969), and this may be the first description of $\omega\langle a\rangle$ slip in naturally deformed quartz.

5.2. Fast growth and locking up of kink bands

The c-axis rotation by kinking in the veins is mostly smaller than 30° (Fig. 6). Kink band structures are always overprinted by recrystallization microstructures in the layer-parallel veins. These phenomena may imply 'fast growth' and 'locking up' of kink bands (Ramsay, 1967; Reches and Johnson, 1976; Weiss, 1980) during deformation. These authors interpreted the mechanism of fast growth and locking up of kink bands from the viewpoint of geometrical strain softening and hardening. When a slip plane in a crystal is inclined at an angle α to the compression axis and the slip direction oriented optimally for slip, the shear stress τ resolved in the slip direction on the layer is expressed as a function of the axial stress σ and inclination angle α as follows:

$$\tau = \sigma \sin\alpha \cos\alpha. \quad (1)$$

The relationship between the values of the ratio σ/τ and inclination angle α is shown in Fig. 9(a). If the anisotropic layer is (sub-)parallel or gently inclined to the compression axis (α_i in Fig. 9a) before deformation, and hence the shear stress resolved on the layer is very small, the axial stress must be very high to initiate kinking (i in Fig. 9a). The required axial stress for kinking becomes smaller as the slip plane in

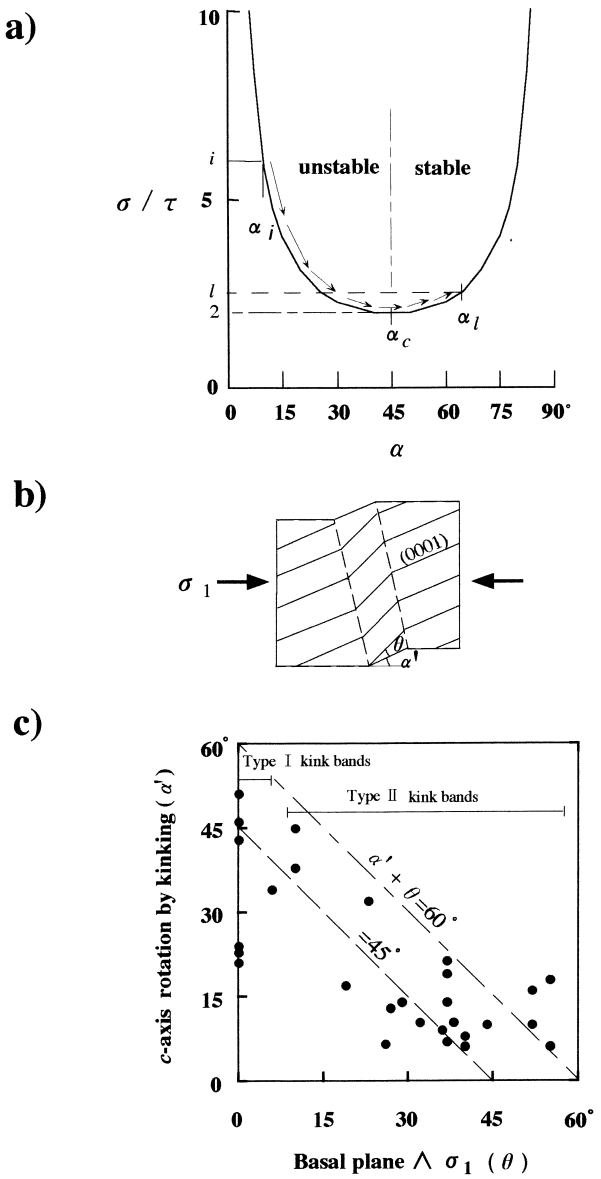

Fig. 9. (a) Relationship between the ratio of axial stress (σ) to resolved shear stress on a slip plane (τ), σ/τ and inclination angle of the slip plane in kink bands (α) to the compression axis. Arrows indicate the change of σ/τ with increasing inclination angle within kink bands. (b) A schematic diagram showing initial inclination angle of basal plane to the compression axis (θ) and rotation angle of basal (0001) plane by kinking (α'). (c) Diagram showing the rotation angle of host c-axis by kinking (α') versus initial inclination angle of basal plane to the compression axis (θ) for kinked host grains from a layer-parallel vein.

kink bands rotates with increasing strain towards the normal to the compression axis (i.e. strain softening, $d\sigma/d\alpha < 0$). Such a deformation could be 'unstable' and the slip plane can rotate quickly by kinking until the optimum inclination angle (45°; α_c in Fig. 9a) for slip is reached. When the inclination angle of the slip plane in kink bands exceeds the angle α_c, the axial stress must increase for further slip to occur on the plane (i.e. $d\sigma/d\alpha > 0$, strain hardening). Therefore, the kinking process slows down leading to the termination of lattice rotation at a certain locking angle (α_l in Fig. 9a).

Consider the locking up of kink bands in the quartz veins assuming that basal slip is the sole active slip system. When the initial and final inclination angles of an anisotropic layer (basal plane) relative to the compression axis are defined as θ and α, respectively, $\alpha' = \alpha - \theta$ is the rotation angle of *c*-axis in kink bands (Fig. 9b). The rotation angles α' in host grains from a gently folded layer-parallel vein are plotted as a function of the initial angles θ in Fig. 9(c). We measured the angles in the hinge of the fold, so that the lattice rotation due to the folding is minimized. Many data are plotted between two lines expressing $\alpha = 45°$ and 60°, respectively, being consistent with the theoretical prediction.

5.3. Evolution of microstructures in the deformed quartz

We inferred the evolution of deformation and recrystallization microstructures in the quartz under subgreenschist conditions as follows (Fig. 10). At the first stage of deformation, under a critical condition for yielding between the anisotropic layers (basal (0001) plane in this case), kink bands begin to form sub-parallel to the *c*-axis orientation, and the active slip plane in kink bands rapidly rotates towards the normal to the shortening axis (the first and the second rows of Fig. 10). Lattice rotation in kink bands stops at some angle of the *c*-axis orientation relative to the shortening axis, exceeding 45° (the second row of Fig. 10). Polygonization and recrystallization via progressive misorientation occur at first preferentially in the highly strained portions such as inside of kink bands,

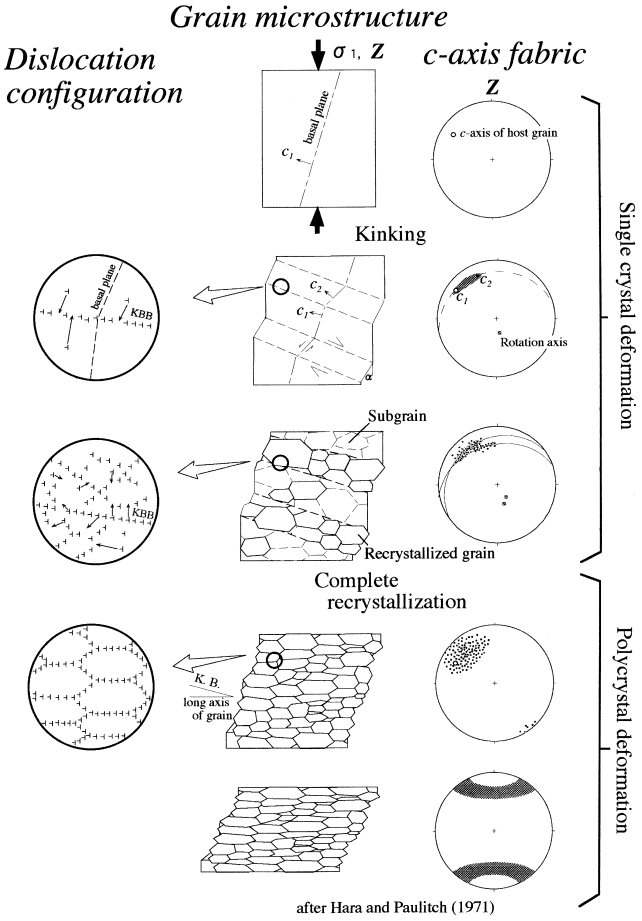

Fig. 10. Schematic diagrams showing the evolutionary process of deformation and recrystallization microstructures in the quartz deformed under subgreenschist conditions, assuming the sole activation of a basal slip system. See text for detailed explanations. KBB: kink band boundary.

and later outside of them (the third row of Fig. 10). In the kinked grain (samples *E*-1–5, *L*1 and 2), COD patterns suggesting the operation of a single slip system are observed. On the other hand, the composite dispersion patterns of crystallographic orientation (observed in samples *E*-6 and *L*-3) probably due to a combination of each misorientation process by subgrain rotation in host domains differently orientated by kinking (the third row of Fig. 10). Subgrains and recrystallized grains are always elongated perpendicular to the finite shortening axis. The independence of the shape fabric of subgrains and recrystallized grains on pre-formed structures such as kink bands and host crystallographic orientations (i.e. the orientation of the active slip plane) suggests that rotation recrystallization results from a complete rearrangement of dislocation configuration by climbing (the third and fourth rows of Fig. 10). This conclusion is also supported by pervasive development of dislocation walls in the quartz grains (Fig. 7b).

COD of recrystallized grains becomes less systematic leading to the complicated (or random) patterns (observed in samples *L*-4 and *L*-5) as subgrain rotation recrystallization progresses further (i.e. misorientation angles increase) and kink band structures disappear (the fourth row of Fig. 10; cf. Takeshita and Hara, 1998). Further deformation could be accommodated by polycrystalline deformation. In this stage, grain boundary migration would become an important recrystallization mechanism, since the mobility of grain boundaries increases with progressive misorientation (e.g. Urai et al., 1986; Trimby et al., 1998). In fact, the serrated host grain boundaries shown in Fig. 2(a) suggest the occurrence of grain boundary migration on high-angle boundaries. Hara and Paulitsch (1971) reported a *c*-axis fabric characterized by ca 35° small circle girdles around the *Z*-axis in recrystallized grains from the layer-parallel veins, which could represent a *c*-axis fabric in a more strained state than analyzed in this study (the fifth row of Fig. 10). The small circle girdle *c*-axis fabrics were perhaps formed by lattice rotation in the recrystallized grains accompanying intracrystalline slip under constrained deformation (e.g. Lister et al., 1978). Hence, it could be concluded that with increasing strain, the mode of deformation in the quartz veins changed from that of single crystals represented by kinking, polygonization and rotation recrystallization, to that of polycrystals, where deformation of each recrystallized grain is constrained by that of neighbouring grains and grain boundary migration might pervasively occur.

The microstructural features suggesting pervasive operation of recovery and rotation recrystallization in the quartz veins can be correlated to those of Regime 2 rather than Regime 1 after Hirth and Tullis (1992), although the deformation temperatures estimated from homogenization temperatures of fluid inclusions in the quartz were very low ($T = 250$–350°C) for intracrystalline plasticity in quartz. The layer-parallel veins are in general more strained than the en échelon veins: the stages of deformation and recrystallization in the en échelon and layer-parallel veins correspond with those from the first to third, and from the first to fifth rows of Fig. 10, respectively. Based on the dislocation density, subgrain and recrystallized grain sizes (Table 1), the layer-parallel veins suffered a lower differential stress than the en échelon veins, suggesting a higher deformation temperature in the former than in the latter. Therefore, the reason that the layer-parallel veins suffered more strain and recrystallization than the en échelon veins may have been the slightly higher deformation temperatures as well as the longer duration of deformation in the former veins.

6. Conclusions

1. In both the layer-parallel and the en échelon quartz veins deformed under subgreenschist conditions, kinking caused by basal (0001) slip was a principal deformation mode. Conjugate kink bands (type I) are formed in grains with *c*-axes (sub-)parallel to the shortening axis, while monoclinic bands (type II) are formed in grains with *c*-axes inclined to the shortening axis.
2. The host orientation controlled crystallographic orientation distribution (COD) patterns of subgrain and recrystallized grains revealed that the main dynamic recrystallization mechanism was subgrain rotation. The lattice dispersion patterns suggest the dominant activation of basal $\langle a \rangle$ and $\langle m \rangle$ and subordinate activation of ω $\{10\bar{1}3\}\langle a \rangle$ slip systems.
3. Kink bands in the quartz grains tended to be rotated rapidly and lock up when the angle between the basal plane and the shortening axis is between 45° and 60°. This could be interpreted as resulting from the change in the resolved shear stress on the slip plane with increasing strain, which first increases (strain softening) and then decreases (strain hardening) as the slip plane in kink bands rotates towards the normal orientation to the shortening axis via the optimal orientation ($\alpha = 45°$).
4. The progressive microstructural development from kinking through polygonization to recrystallization in the deformed quartz is reflected in the change of crystallographic orientation distribution from systematic to complicated or random dispersion patterns. The long axes of subgrains and recrystallized grains in the deformed quartz are always perpendicular to the shortening axis regardless of the orientations of host crystals (i.e. active slip plane) and preformed structures (i.e. kink bands). The

grain shape fabric could suggest that the pre-existing dislocation substructures were completely rearranged by dislocation climb during polygonization and subgrain rotation recrystallization in the quartz.

Acknowledgements

We would like to thank T. G. Blenkinsop, G. E. Lloyd and P. W. Trimby for constructive comments for improvement of the manuscript. We wish to thank J.-I. Ando, T. Nagase and H.-R. Wenk for much helpful advice on the TEM observation technique. We thank K. Otsuki for critical reading of an early version of the manuscript and useful comments. We also express gratitude to M. Shishido and J. Nemoto for their help in making thin sections and photographs. We are particularly grateful to the late A. Minami for technical assistance in TEM observation.

References

Ave'Lallemant, H.G., Carter, N.L., 1971. Pressure dependence of quartz deformation lamellae orientations. American Journal of Science 270, 218–235.

Baëta, R.D., Ashbee, K.H.G., 1969. Slip systems in quartz, I, Experiments. American Mineralogist 54, 1551–1573.

Banno, S., Sakai, C., 1989. Geologic and metamorphic evolution of the Sanbagawa metamorphic belt, Japan. In: Daly, J.S., Cliff, R.A., Yardley, B. (Eds.), Evolution of Metamorphic Belts, Geological Society of London Special Publication, 43. Blackwell Scientific Publications, Oxford, pp. 519–532.

Bouchez, J.-L., 1977. Plastic deformation of quartzites at low temperature in area of natural strain gradient. Tectonophysics 39, 25–50.

Carter, N.L., Friedman, M., 1965. Dynamic analysis of deformed quartz and calcite from the Dry Creek Ridge Anticline, Montana. American Journal of Science 263, 747–785.

Faure, M., 1985. Microtectonic evidence for eastward ductile shear in the Jurassic orogen of SW Japan. Journal of Structural Geology 7, 175–186.

Fliervoet, T.E., White, S.H., 1995. Quartz deformation in a very fine grained quartzo-feldspathic mylonite: a lack of evidence for dominant grain boundary sliding deformation. Journal of Structural Geology 17, 1095–1109.

Gleason, G.C., Tullis, J., Heidelbach, F., 1993. The role of dynamic recrystallization in the development of lattice preferred orientations in experimentally deformed quartz aggregates. Journal of Structural Geology 15, 1145–1168.

Hara, I., Paulitsch, P., 1971. c-Axis fabrics of quartz in buckled quartz veins. Neues Jahrbuch fur Mineralogie Abhandlungen 155, 31–53.

Hara, I., Hide, K., Takeda, K., Tsukuda, E., Tokuda, M., Shiota, T., 1977. Tectonic movement in the Sambagawa belt. In: Hide, K. (Ed.), The Sambagawa Belt. Hiroshima University Press, Hiroshima, pp. 309–390 (in Japanese with English abstract).

Hara, I., Shiota, T., Hide, K., Kanai, K., Goto, M., Seki, S., Kaikiri, K., Takeda, K., Hayasaka, Y., Miyamoto, T., Sakurai, Y., Ohtomo, Y., 1992. Tectonic evolution of the Sambagawa schists and its implications in convergent margin processes. Journal of Science of Hiroshima University Series C 9, 495–595.

Hirth, G., Tullis, J., 1992. Dislocation creep regimes in quartz aggregates. Journal of Structural Geology 14, 145–159.

Isozaki, Y., Itaya, T., 1990. Chronology of Sanbagawa metamorphism. Journal of Metamorphic Geology 8, 401–411.

Kawato, K., Isozaki, Y., Itaya, T., 1991. Geotectonic boundary between the Sanbagawa and Chichibu belts in central Shikoku, Southwest Japan. Journal of Geological Society of Japan 97, 959–975 (in Japanese with English abstract).

Law, R.D., Schmid, S.M., Wheeler, J., 1990. Simple shear deformation and quartz crystallographic fabric: a possible natural example from the Torridon area of NW Scotland. Journal of Structural Geology 12, 29–45.

Lister, G.S., Paterson, M.S., Hobbs, B.E., 1978. The simulation of fabric development in plastic deformation and its application to quartzite: the model. Tectonophysics 45, 107–158.

Lloyd, G.E., Freeman, B., 1991. SEM electron channeling analysis of dynamic recrystallization in a quartz grain. Journal of Structural Geology 13, 945–953.

Lloyd, G.E., Freeman, B., 1994. Dynamic recrystallization of quartz under greenschist conditions. Journal of Structural Geology 16, 867–881.

Lloyd, G.E., Farmer, A.B., Mainprice, D., 1997. Misorientation analysis and formation and orientation of subgrain and grain boundaries. Tectonophysics 279, 55–78.

Lloyd, G.E., Law, R.D., Mainprice, D., Wheeler, J., 1992. Microstructural and crystal fabric evolution during shear zone formation. Journal of Structural Geology 14, 1079–1100.

Nicolas, A., Poirier, J.P., 1976. In: Crystalline Plasticity and Solid State Flow in Metamorphic Rocks. Wiley, London.

Nishikawa, O., Takeshita, T., 1999. Dynamic analysis and two types of kink bands in quartz veins deformed under subgreenschist conditions. Tectonophysics 301, 21–34.

Nishikawa, O., Misawa, T., Ogawa, S., Otsuki, K., 1994. Structural analysis of low grade metamorphic rocks of Sambagawa Belt in central Shikoku, Japan. Journal of Geological Society of Japan 100, 901–914 (in Japanese with English abstract).

Ramsay, J.G., 1967. In: Folding and Fracturing of Rocks. McGraw-Hill, New York.

Reches, Z., Johnson, A.M., 1976. Asymmetric folding and monoclinal kinking. Tectonophysics 35, 295–334.

Schmid, S.M., Casey, M., 1986. Complete fabric analysis of some commonly observed quartz *c*-axis patterns. In: Hobbs, B.E., Heard, H.C. (Eds.), Mineral and Rock Deformation: Laboratory Studies (The Paterson volume), Geophysical Monograph Series 36. American Geophysical Union, Washington DC, pp. 263–286.

Seki, S., Hara, I., Shiota, T., 1993. Transition from flexural-flow folding to flexural-slip folding in the Sambagawa belt. Journal of Science of Hiroshima University Series C4, 685–696.

Takeshita, T., Hara, I., 1998. c-Axis fabrics and microstructures in a recrystallized quartz veins deformed under fluid-rich greenschist conditions. Journal of Structural Geology 20, 417–431.

Takeshita, T., Wenk, H.-R., 1988. Plastic anisotropy and geometrical hardening in quartzites. Tectonophysics 149, 345–361.

Takeshita, T., Naomoto, K., Yagi, K., 1997. Studies on the deformed rock samples collected by Department of Earth and Planetary Systems Science, Hiroshima University, part 3: Dynamic analysis of deformed quartz grains in en échelon quartz veins and their formation temperatures. Bulletin of Hiroshima University Museum No. 3, 41–49 (in Japanese with English abstract).

Takeshita, T., Wenk, H.-R., Lebensohn, R., 1999. Development of preferred orientation and microstructure in sheared quartzite: comparison of natural data and simulated results. Tectonophysics (in press).

Trépied, L., Doukhan, J.C., Paquet, J., 1980. Subgrain boundaries in quartz. Theoretical analysis and microscopic observations. Physics and Chemistry of Minerals 5, 201–218.

Trimby, P.W., Prior, D.J., Wheeler, J., 1998. Grain boundary hierarchy development in quartz mylonite. Journal of Structural Geology 20, 917–935.

Tullis, J., Dell'Angelo, L., Yund, R.A., 1990. Ductile shear zones from brittle precursors in feldspathic rocks: The role of dynamic recrystallization. In: Duba, A.G., Durham, W.B., Handin, J.W., Wang, H.F. (Eds.), The Brittle–Ductile Transition in Rocks (The Heard Volume), Geophysical Monograph Series 56. American Geophysical Union, Washington DC, pp. 67–81.

Urai, J.L., Means, W.D., Lister, G.S., 1986. Dynamic recrystallization of minerals. In: Hobbs, B.E., Heard, H.C. (Eds.), Mineral and Rocks Deformation: Laboratory Studies (The Paterson volume), Geophysical Monograph Series 36. American Geophysical Union, Washington DC, pp. 161–199.

van Daalen, M., Heilbronner, R., Kunze, K., 1999. Orientation analysis of localized shear deformation in quartz fibers at the brittle–ductile transition. Tectonophysics 303, 83–107.

Weiss, L.E., 1980. Nucleation and growth of kink bands. Tectonophysics 65, 1–38.

White, S.H., 1977. Geological significance of recovery and recrystallization processes in quartz. Tectonophysics 39, 143–170.